In-Plane Optical Anisotropy and Linear Dichroism in Low-Symmetry Layered TlSe

Shengxue Yang,[†,#] *Chunguang Hu,*[‡, #] *Minghui Wu,*[§, #] *Wanfu Shen,*[‡, #] *Sefaattin Tongay,*[∥] *Kedi Wu,*[∥] *Bin Wei,*[⊥] *Zhaoyang Sun,*[‡] *Chengbao Jiang,*[*,†] *Li Huang,*[*, §] *Zhongchang Wang*[*,⊥]

[†]School of Materials Science and Engineering, Beihang University, Beijing 100191, P. R. China

[‡]State Key Laboratory of Precision Measuring Technology and Instruments, Tianjin University, Weijin Road, CN-300072 Tianjin, P. R. China

[§] Department of Physics, Southern University of Science and Technology, Shenzhen 518005, P. R. China

[∥]School for Engineering of Matter, Transport and Energy, Arizona State University, Tempe, AZ 85287, United States

[⊥] Department of Quantum and Energy Materials, International Iberian Nanotechnology Laboratory (INL), Av. Mestre José Veiga s/n, Braga 4715-330, Portugal

*Corresponding Author:
Prof. Chengbao Jiang
School of Materials Science and Engineering, Beihang University, Beijing 100191, P. R. China
Email: jiangcb@buaa.edu.cn

Prof. Li Huang
Department of Physics, South University of Science and Technology of China, Shenzhen 518005, P. R. China
Email: huangl@sustc.edu.cn

Prof. Zhongchang Wang
Department of Quantum and Energy Materials, International Iberian Nanotechnology Laboratory (INL), Av. Mestre José Veiga s/n, Braga 4715-330, Portugal
Email: zhongchang.wang@inl.int

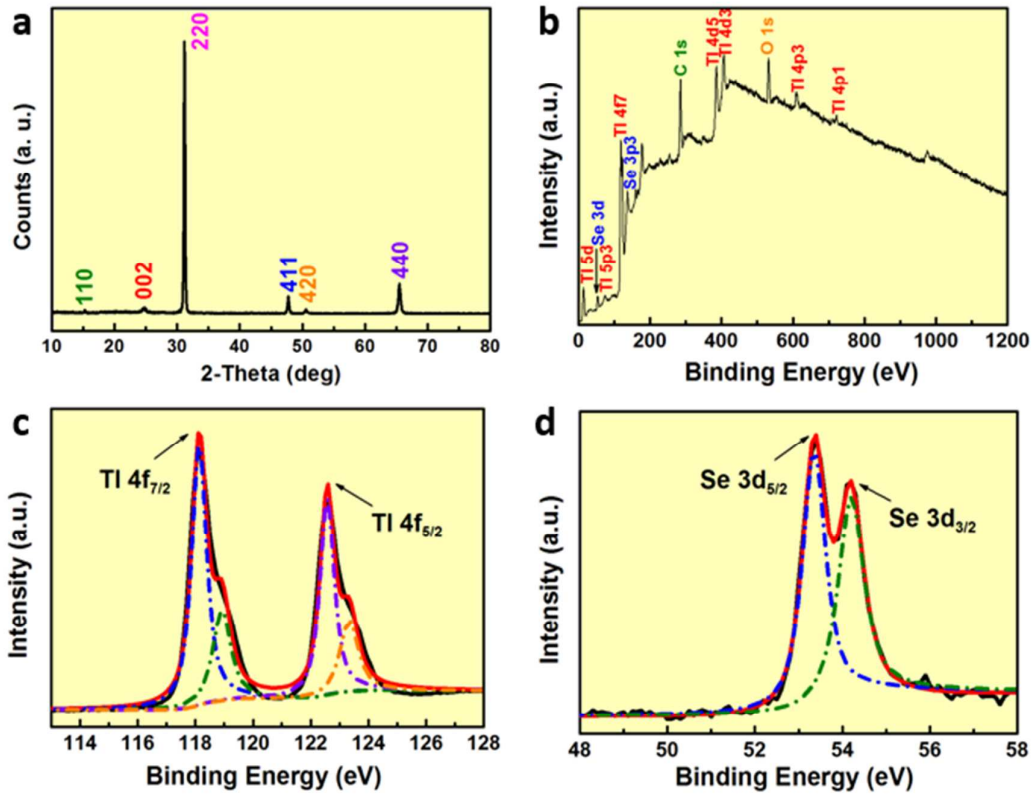

Figure S1. (a) XRD pattern of TlSe single crystals. (b) XPS full spectrum of bulk TlSe. The high-solution XPS signals of Tl 4f (c) and Se 3d (d).

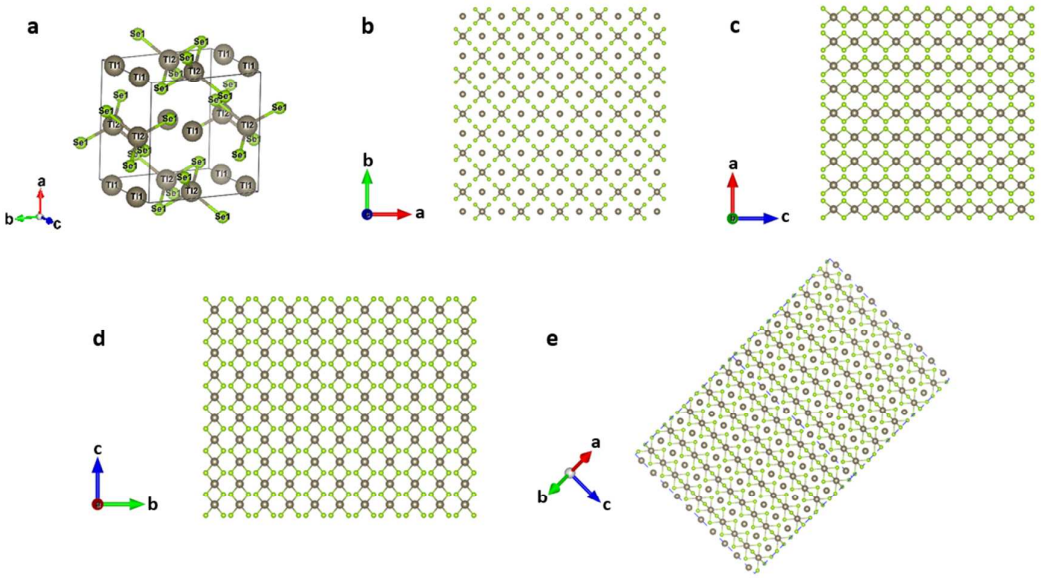

Figure S2. (a) The conventional cell of bulk TlSe. Top view (b) and side views (c-e) of TlSe crystal structure.

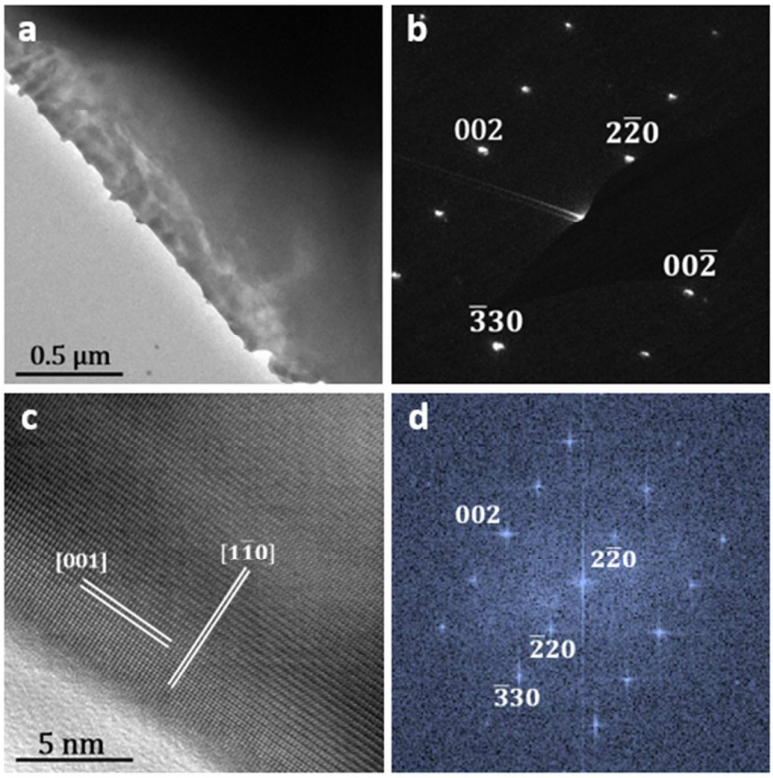

Figure S3. (a) TEM image of a thin area of the mechanically exfoliated TlSe flake. (b) SADP, (c) HRTEM image and (d) FFT image of this flake.

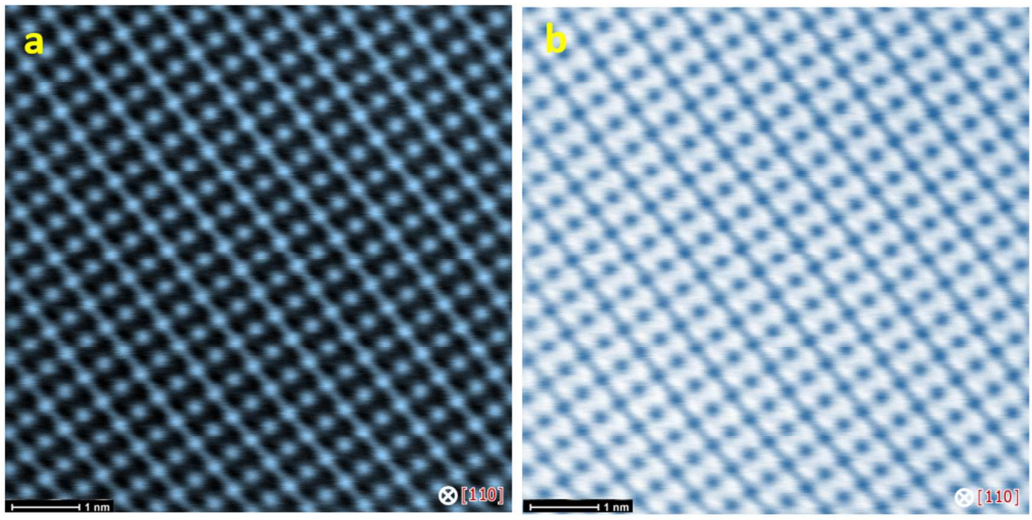

Figure S4. Atomic-resolution HAADF (a) and BF STEM (b) images viewed from [110] direction.

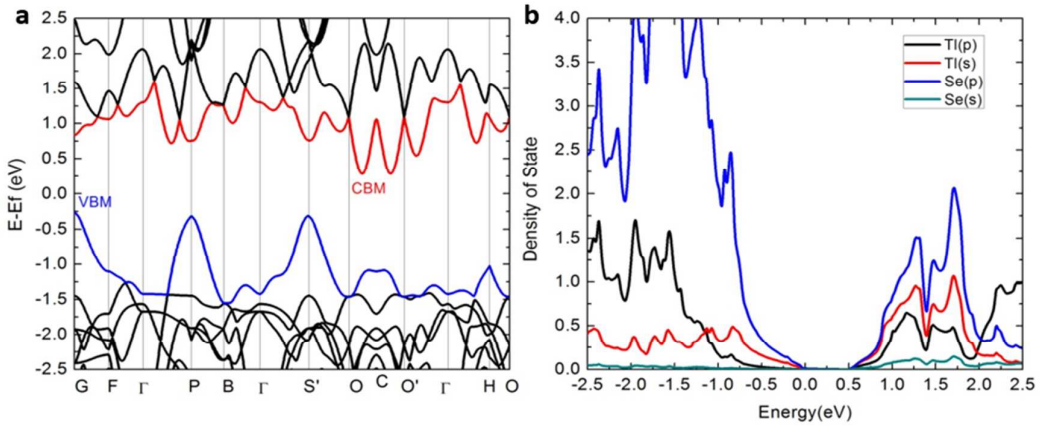

Figure S5. (a) Band structure and (b) partial density of state (PDOS) of bulk TlSe.

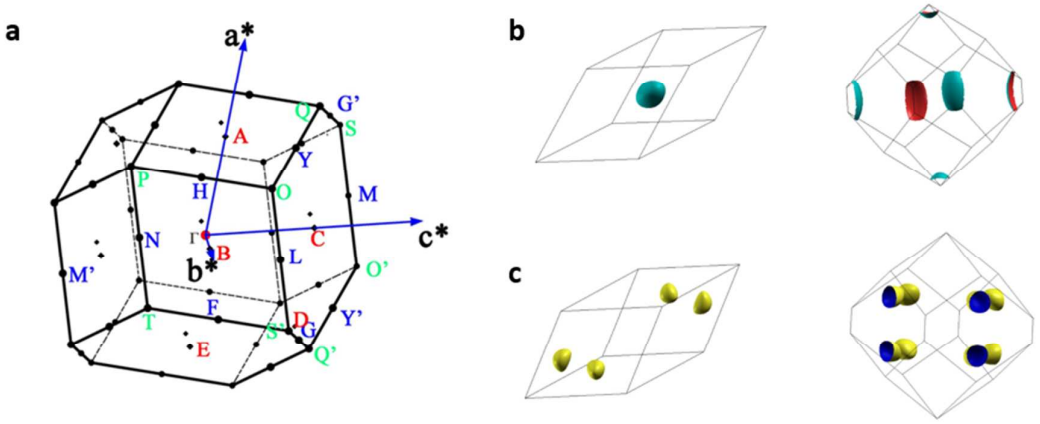

Figure S6. (a) The first Brillouin zone (BZ) of bulk TlSe with high-symmetry points. Fermi surface around VBM (b) and CBM (c) is about 0.2 eV. The left of the figure shows the Fermi surface in the reciprocal unite cell and the right of the figure is the first BZ.

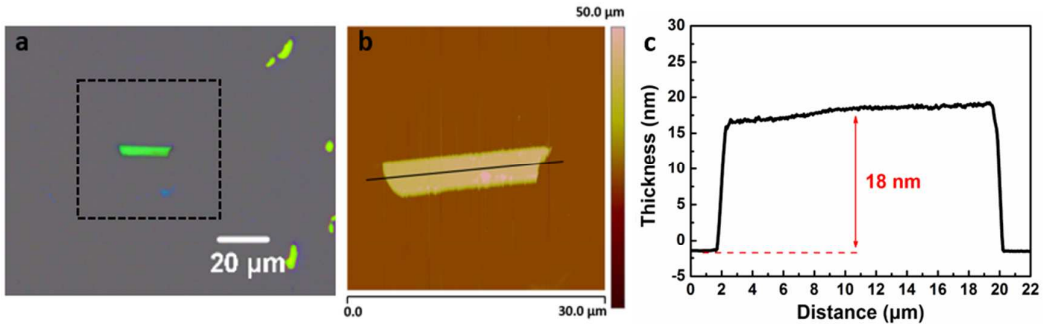

Figure S7. (a) The optical image of few-layer TlSe flakes on a Si wafer with a 300 nm SiO_2 layer. (b) AFM image of a typical TlSe flake. (c) The corresponding cross-section scan along the black line in b.

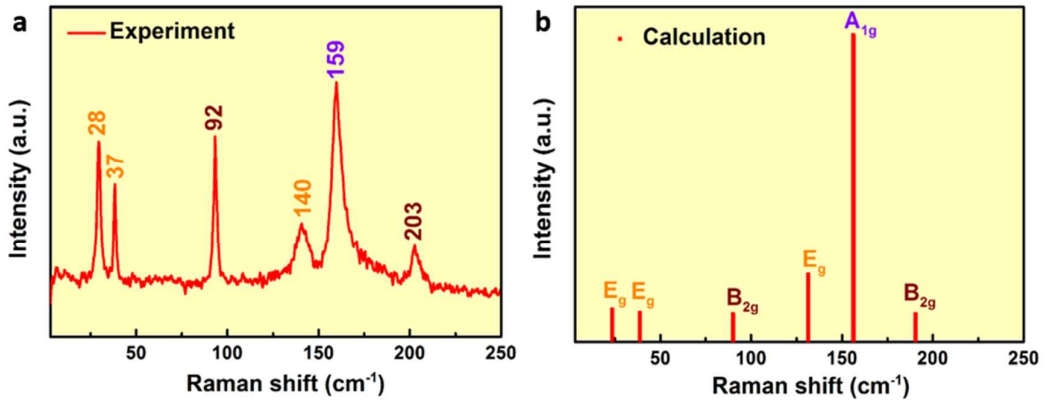

Figure S8. (a) Unpolarized Raman spectrum of an 18-nm TlSe flake at excitation wavelength of 633 nm. (b) The Raman intensity of bulk TlSe calculated by the DFT methods.

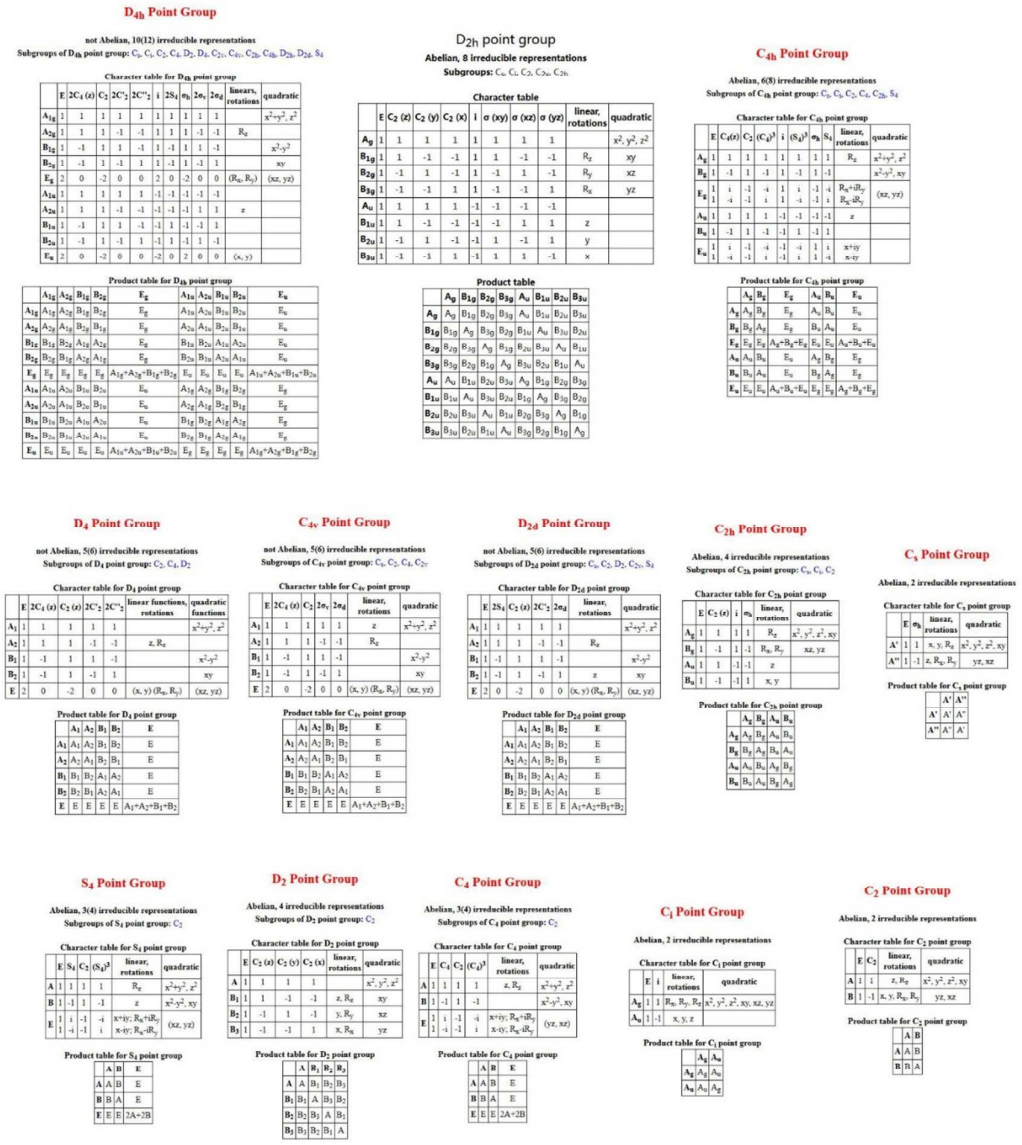

Figure S9. Character table of D_{4h} and its subgroups.

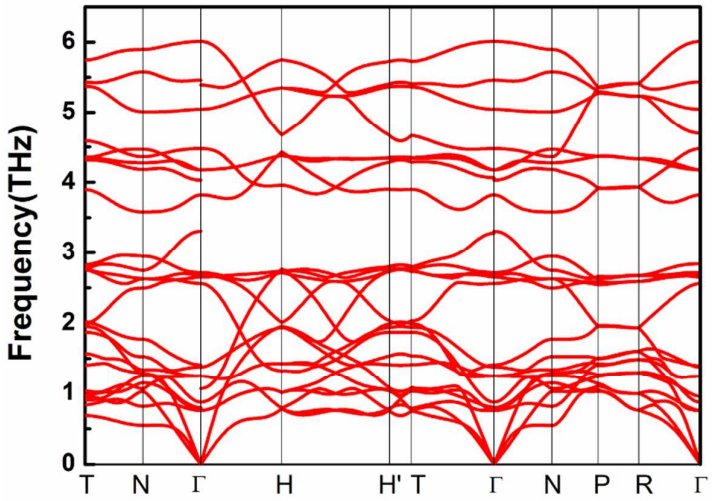

Figure S10. TlSe phonon dispersion with the correction of long range interaction of macroscopic electric field induced by polarization of collective ionic motion near Gamma point.

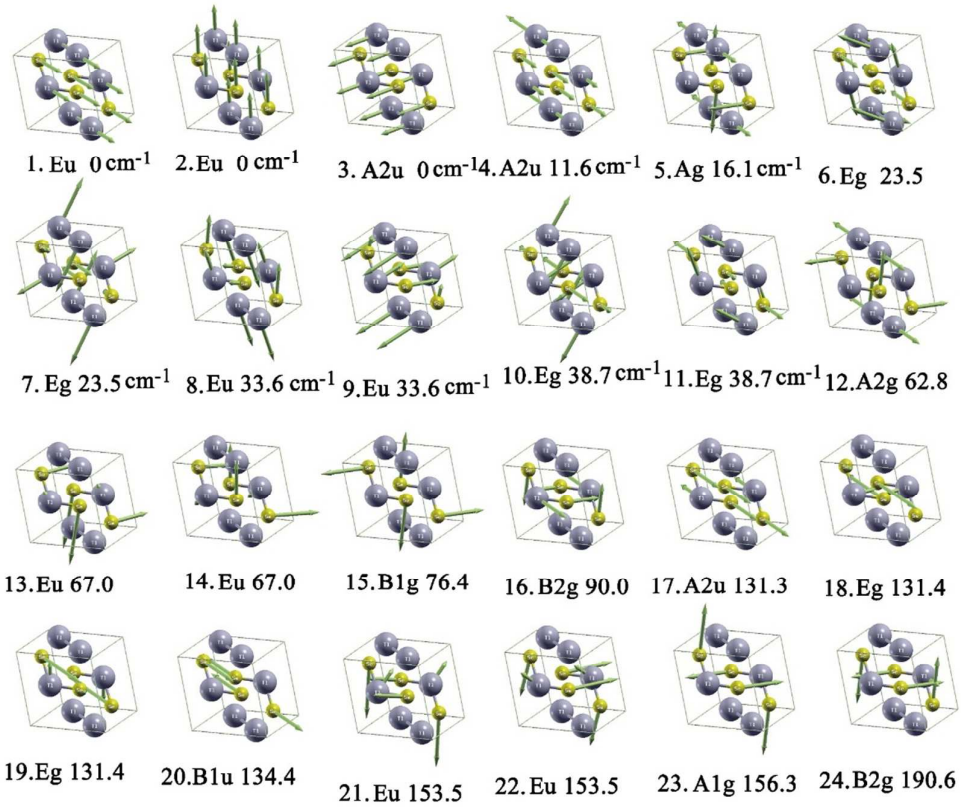

Figure S11. Atom moving directions of phonon modes at Gamma point for bulk TlSe.

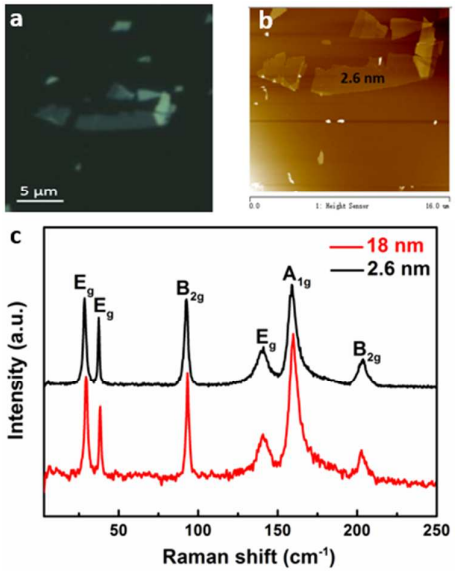

Figure 12. (a) Optical image of a 2.6-nm TlSe flake. (b) AFM image of this flake. (c) The comparison of Raman spectra for two flakes with different thicknesses (18 nm and 2.6 nm).

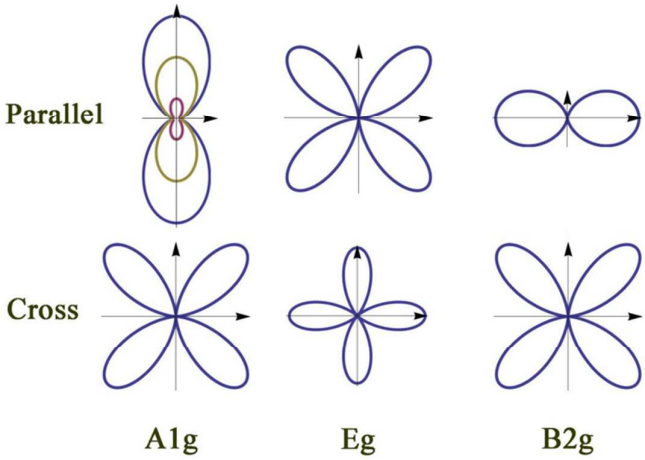

Figure S13. Possible patterns of polar plots for anisotropic Raman intensities simulated according to the Raman tensor.

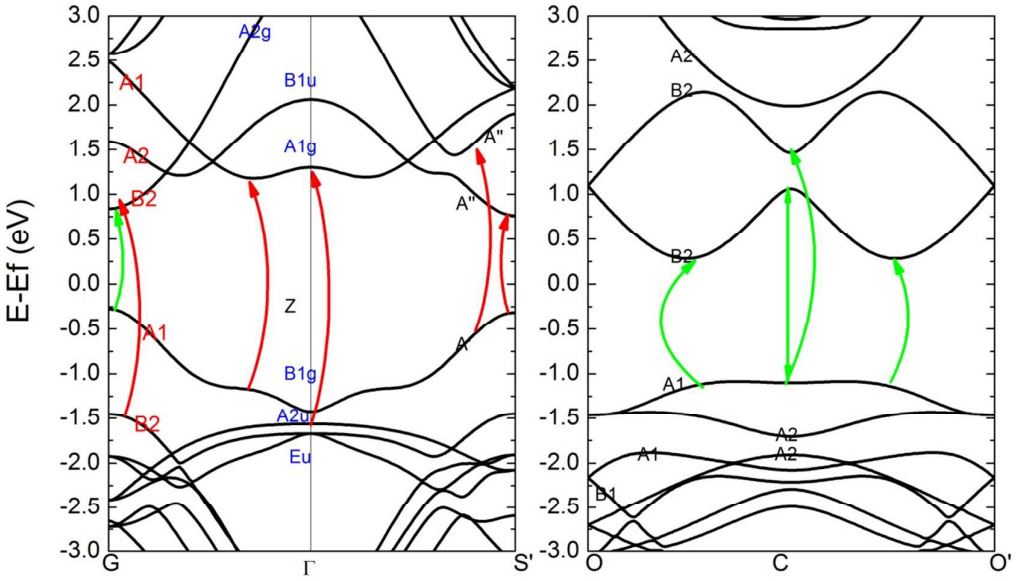

Figure S14. HSE06 obtained band structure of TlSe, the red lines denote the possible [001] polarized light jump, while green lines denote the jump of [1$\bar{1}$0] polarized light.

Table S1 Selection rule for A_{2u} Polarization light, [001]-direction.

A_{2u}, H_{oe}		E_g phonon		B_{2g} phonon		A_{1g} phonon	
		$H_{ep}(E_g)$	$H_{oe}(A_{2u})$	$H_{ep}(B_{2g})$	$H_{oe}(A_{2u})$	$H_{ep}(A_{1g})$	$H_{oe}(A_{2u})$
$\|i\rangle$	$\|m'\rangle$	$\|m\rangle$	$\|f\rangle$	$\|m\rangle$	$\|f\rangle$	$\|m\rangle$	$\|f\rangle$
$A_{1g}(\Gamma1)$	A_{2u}	E_u	E_g	B_{1u}	B_{2g}	A_{2u}	A_{1g}
$A_{2g}(\Gamma2)$	A_{1u}	E_u	E_g	B_2u	B_{1g}	A_{1u}	A_{2g}
$B_{1g}(\Gamma3)$	B_{2u}	E_u	E_g	A_{1u}	A_{2g}	B_{2u}	B_{1g}
$B_{2g}(\Gamma4)$	B_{1u}	E_u	E_g	A_{2u}	A_{1g}	B_{1u}	B_{2g}
$E_g(\Gamma5)$	E_u	$A_{1u}+A_{2u}+B_{1u}+B_{2u}$	$A_{1g}+A_{2g}+B_{1g}+B_{2g}$	E_u	E_g	E_u	E_g
$A_{1u}(\Gamma6)$	A_{2g}	E_g	E_u	B_{1g}	B_{2u}	A_{2g}	A_{1u}
$A_{2u}(\Gamma7)$	A_{1g}	E_g	E_u	B_{2g}	B_{1u}	A_{1g}	A_{2u}
$B_{1u}(\Gamma8)$	B_{2g}	E_g	E_u	A_{1g}	A_{2u}	B_{2g}	B_{1u}
$B_{2u}(\Gamma9)$	B_{1g}	E_g	E_u	A_{2g}	A_{1u}	B_{1g}	B_{2u}
$E_u(\Gamma10)$	E_g	$A_{1g}+A_{2g}+B_{1g}+B_{2g}$	$A_{1u}+A_{2u}+B_{1u}+B_{2u}$	E_g	E_u	E_g	E_u

Table S2 Selection rule for E_u Polarization light, [1 -1 0] direction.

E_u, H_{oe}		E_g phonon		B_{2g} phonon		A_{1g} phonon	
		$H_{ep}(E_g)$	$H_{oe}(E_u)$	$H_{ep}(B_{2g})$	$H_{oe}(E_u)$	$H_{ep}(A_{1g})$	$H_{oe}(E_u)$
$\|i\rangle$	$\|m'\rangle$	$\|m\rangle$	$\|f\rangle$	$\|m\rangle$	$\|f\rangle$	$\|m\rangle$	$\|f\rangle$
A_{1g}	E_u	$A_{1u}+A_{2u}+B_{1u}+B_{2u}$	E_g	E_u	$A_{1g}+A_{2g}+B_{1g}+B_{2g}$	E_u	$A_{1g}+A_{2g}+B_{1g}+B_{2g}$
A_{2g}	E_u	$A_{1u}+A_{2u}+B_{1u}+B_{2u}$	E_g	E_u	$A_{1g}+A_{2g}+B_{1g}+B_{2g}$	E_u	$A_{1g}+A_{2g}+B_{1g}+B_{2g}$
B_{1g}	E_u	$A_{1u}+A_{2u}+B_{1u}+B_{2u}$	E_g	E_u	$A_{1g}+A_{2g}+B_{1g}+B_{2g}$	E_u	$A_{1g}+A_{2g}+B_{1g}+B_{2g}$
B_{2g}	E_u	$A_{1u}+A_{2u}+B_{1u}+B_{2u}$	E_g	E_u	$A_{1g}+A_{2g}+B_{1g}+B_{2g}$	E_u	$A_{1g}+A_{2g}+B_{1g}+B_{2g}$
E_g	$A_{1u}+A_{2u}+B_{1u}+B_{2u}$	E_u	$A_{1g}+A_{2g}+B_{1g}+B_{2g}$	$A_{1u}+A_{2u}+B_{1u}+B_{2u}$	E_g	$A_{1u}+A_{2u}+B_{1u}+B_{2u}$	E_g
A_{1u}	E_g	$A_{1g}+A_{2g}+B_{1g}+B_{2g}$	E_u	E_g	$A_{1u}+A_{2u}+B_{1u}+B_{2u}$	E_g	$A_{1u}+A_{2u}+B_{1u}+B_{2u}$
A_{2u}	E_g	$A_{1g}+A_{2g}+B_{1g}+B_{2g}$	E_u	E_g	$A_{1u}+A_{2u}+B_{1u}+B_{2u}$	E_g	$A_{1u}+A_{2u}+B_{1u}+B_{2u}$
B_{1u}	E_g	$A_{1g}+A_{2g}+B_{1g}+B_{2g}$	E_u	E_g	$A_{1u}+A_{2u}+B_{1u}+B_{2u}$	E_g	$A_{1u}+A_{2u}+B_{1u}+B_{2u}$
B_{2u}	E_g	$A_{1g}+A_{2g}+B_{1g}+B_{2g}$	E_u	E_g	$A_{1u}+A_{2u}+B_{1u}+B_{2u}$	E_g	$A_{1u}+A_{2u}+B_{1u}+B_{2u}$
E_u	$A_{1g}+A_{2g}+B_{1g}+B_{2g}$	E_g	$A_{1u}+A_{2u}+B_{1u}+B_{2u}$	$A_{1g}+A_{2g}+B_{1g}+B_{2g}$	E_u	$A_{1g}+A_{2g}+B_{1g}+B_{2g}$	E_u

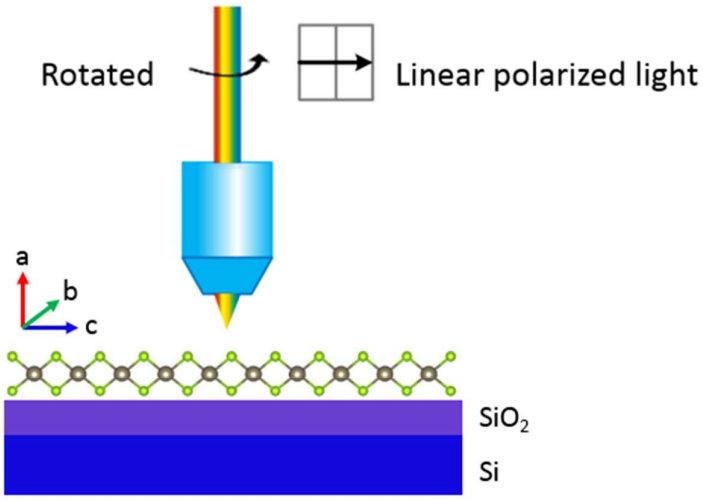

Figure S15. Schematic diagram of the ADRDM measurement.

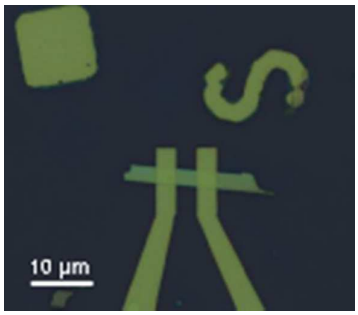

Figure S16. The optical image of a typical TlSe two-terminal device.

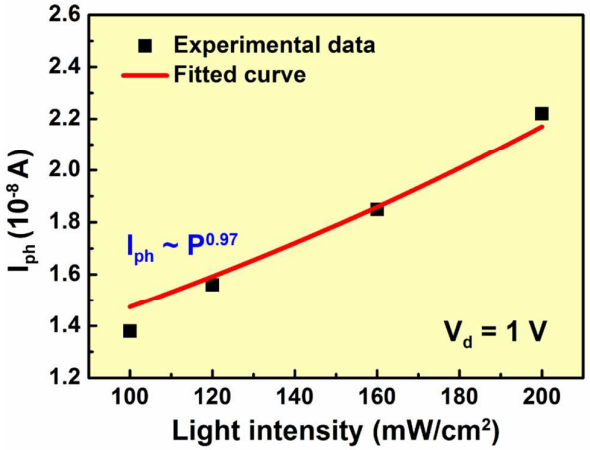

Figure S17. Experimental data fitting of photocurrent curves as changing of light intensities shown in Figure 5b.

Analysis of Raman anisotropy

The one-step Raman spectroscopy contains three micro-steps: (1) An electron absorbs a photon and jumps into a high energy level state. The scattering matrix of this process can be described as $\langle m|H_{eo}|i\rangle$, where H_{eo} is the Hamiltonian of electron-photon interaction. At first-order approximation, H_{eo} can be described as

$$H_{eo} = -\frac{e}{mc}\mathbf{A}(\mathbf{r})\cdot\mathbf{P} \tag{1}$$

where c is the speed of light, $\mathbf{A}(\mathbf{r})$ is the vector potential of optical electromagnetic field and $\mathbf{P}$ is the momentum of electron. As the vector potential is an external field, the Schrödinger group is determined by $\mathbf{P}$; (2) An excitation electron interacts with a phonon. In one-step Raman spectroscopy, only the phonon nearby the center zone can be involved into the electron-photon interaction. The scattering matrix of this process can be described as $\langle m'|H_{ep}|m\rangle$, where H_{ep} is the Hamiltonian of electron-phonon interaction, which can be expressed as

$$H_{ep} = \Delta V(\mathbf{r}) \tag{2}$$

where ΔV is the change of potential caused by the phonon vibration. It is obvious that the Schrödinger group of this Hamiltonian follows the symmetry of corresponding phonon mode; (3) The last step is also an electron-photon interaction process, in which the excitation electron emits a photo when jumping into a low energy level state. The expression of Hamiltonian is same as the first step. In summary, the whole process of one-step Raman spectroscopy based on the Fermi-Gold rule can be described as,

$$I_\nu(E_L) = \left| \sum_{i,m,m'} \frac{\langle f|H_{op}|m'\rangle\langle m'|H_{ep}^{\nu}|m\rangle\langle m|H_{op}|i\rangle}{(E_L - \Delta E_{mi})(E_L - \hbar\omega_\nu - \Delta E_{m'i})} \right|^2 \tag{3}$$

where I is the scattering strength, $\Delta E_{mi} = E_m - E_i - i\Gamma$, $m(m')$ represents the intermediate state and Γ is a broadening factor, corresponding to the lifetime of photo-excited electrons.

For the active Raman modes in TlSe, their Raman tensor R can be expressed as follows

$$R\left(\mathrm{A_{1g}}\right)=\begin{pmatrix} a\cdot e^{i\phi_a} & 0 & 0 \\ 0 & b\cdot e^{i\phi_b} & 0 \\ 0 & 0 & \mathrm{b}\cdot e^{i\phi_b} \end{pmatrix}; \tag{4}$$

$$R\left(\mathrm{B_{2g}}\right)=\begin{pmatrix} 0 & 0 & d\cdot e^{i\phi_d} \\ 0 & d\cdot e^{i\phi_d} & 0 \\ 0 & 0 & 0 \end{pmatrix}; \tag{5}$$

$$R_{\mathrm{1}}\left(\mathrm{E}_g\right)=\begin{pmatrix} 0 & f\cdot e^{i\phi_e} & 0 \\ f\cdot e^{i\phi_e} & 0 & 0 \\ 0 & 0 & 0 \end{pmatrix}. \tag{6}$$

where ϕ_a, ϕ_b, ϕ_d, ϕ_e are phases of Raman tensor elements. The Raman intensity $I\left(j\right)$ of the mode *j* can be expressed as

$$I\left(j\right)\propto\left|\hat{\mathbf{g}}_s\cdot\overline{\overline{R}}\left(j\right)\cdot\hat{\mathbf{g}}_i^T\right|, \tag{7}$$

where $\hat{g}_i$ and $\hat{g}_s$ are the polarized direction of the incident and scattered lights, respectively.

In the parallel configuration, since the angle between $\hat{g}_i$ and $\hat{g}_s$ is 0°, the Raman intensity for A_g mode is described as

$$I^{\mathrm{Para}}\left(\mathrm{A_{1g}}\right)\propto\left(cos^2\left(\theta\right)+\frac{|a|}{|b|}\cdot\sin^2\left(\theta\right)\cdot\cos\phi_{ab}\right)^2+\frac{|a|}{|b|}\sin^4\left(\theta\right)\sin^2\left(\phi_{ab}\right); \tag{8}$$

for B_{2g} mode, it is described as

$$I^{\mathrm{Para}}\left(\mathrm{B_{2g}}\right)\propto\left|d\right|^2\cos^4\left(\theta\right); \tag{9}$$

and for E_g mode, it is described as

$$I^{\text{Para}}\left(\mathrm{E}_g\right) \propto 4|f|^2 \sin^2\left(2\theta\right). \tag{10}$$

In the cross configuration, the angle between $\hat{g}_i$ and $\hat{g}_s$ is 90°, and the Raman intensity for A_g mode is described as

$$I^{\text{Cross}}\left(\mathrm{A}_{1g}\right) \propto \left(|a|-|b|\right)^2 \sin^2\left(\theta\right)\cos^2\left(\theta\right); \tag{11}$$

for B_{2g} mode, it is described as

$$I^{Cross}\left(\mathrm{B}_{2g}\right) \propto |d|^2 \sin^2\left(2\theta\right); \tag{12}$$

and for E_g mode, it is described as

$$I^{Cross}\left(\mathrm{E}_g\right) \propto |f|^2 \cos^2\left(2\theta\right). \tag{13}$$

In all these equations, θ is the angle between the probe direction and x-axis direction of polar plots, and $\phi_{ab} = \phi_a - \phi_b$ defines phase difference. From Eqs. (8) to (13), one can notice that the polar plots depend not only on the configuration but also on the phase difference of Raman tensor. We simulated the polarized Raman intensity based on the Raman tensor, and the possible patterns of polar plots are shown in Figure S12. The calculated curves match well with the experimental ones (Figure 2c). The polar plots of E_g modes are 4-leaf patterns, and the pattern for the cross configuration seems to be rotated by 45° in comparison to that in the parallel configuration. In the parallel configuration, the polar plots of A_{1g} and B_{2g} modes are 2-leaf patterns, while they are changed to 4-leaf patterns under cross configuration.

According to Eq. (8), the $\frac{|a|}{|b|}$ value determines the direction of the main axis: if $\frac{|a|}{|b|}$ >1, the main axis is along the y-direction.